UCRL-TR-218917

LAWRENCE
LIVERMORE
NATIONAL
LABORATORY

Thermal Modeling Tool for a Spherical Capsule in a Sputtering Chamber

A. P. Wemhoff

February 13, 2006

Disclaimer

Abstract

It is known that a film's temperature during a sputtering process greatly influences its mechanical structure. Currently, there is no known tool to effectively model the temperature history of a sputtered film on a spherical capsule in a sputtering chamber. Therefore, a tool has been developed that allows for the prediction of this temperature history using a lumped capacitance approximation for the capsule. This tool has been developed as part of LLNL's Diablo II multi-mechanics code to allow for the coupling of the capsule mechanics with the finite element-based sputtering chamber mechanics. The tool incorporates three forms of heat transfer: contact heat transfer between the capsule and the walls, enclosure radiation among all surfaces, and adsorption of chamber gas on all surfaces. The physics of the system have been validated by determining less than 1% difference in simulated results of twelve test runs to values determined via analytical or finite difference approaches, and validation of eight further tests involving capsule motion provide confidence in the model.

Table of Contents

Introduction

The temperature of a sputtered film on a substrate has been shown to be heavily dependent upon its material properties. Thornton [1] provided an extremely useful discussion of film morphology and its dependence on external conditions. His analysis singles out the argon pressure and normalized substrate temperature as the two accessible parameters to control film morphology. It is clear that operating at low normalized temperature would yield low-density columnar structures, which are undesirable for most applications. Therefore, according to his diagram, dense films composed of materials with high melting points would require high substrate temperatures, and this would limit the applicability of the sputtering method unless high melting point substrates could be used.

There currently is no tool to accurately predict the temperature of a film during a sputtering process, although rough calculations have been performed by Rich London [2], where the temperature of the pan was measured to be 110°C, and a thermocouple suspended 1 cm above the pan measured a temperature of 170°C. The calculations assumed a gun heat output of 200 W/gun for 4 guns, and the contact between the capsule and the pan was assumed to be existent 1% of the time with 1% of the total surface area of the capsule in contact with the pan.

The tool described in this study uses a lumped capacitance approach to predict the volumetrically-averaged, time dependent temperature of the capsule during the sputtering process. The lumped model assumption is validated spatially since the capsule rotates throughout the sputtering process. Furthermore, the film substrate is a hollow plastic shell, and sputtered films are on the order of microns, which suggests nearly uniform film temperature in the radial direction.

In this model, three forms of heat transfer were incorporated: interaction with the chamber gas molecules, contact between the capsule and the chamber walls, and enclosure radiation. Although the gas in the chamber is nearly a vacuum, it is anticipated that the energy gained by adsorption and reflection of the gas molecules on the solid surfaces would be dependent upon the difference of the energies of the impinging gas molecules and the solid molecules on the surface, and thus the interaction would be most appropriately handled by a convection model. The convection implementation is straightforward and will not be discussed further, although it should be mentioned that the assumption exists that the chamber gas replenishes at a rate such that its heat transfer to solid surfaces does not greatly affect its temperature distribution. The implementation of the contact and enclosure radiation algorithms will be discussed later.

The thermal modeling tool was implemented in the LLNL code Diablo II as opposed to creating a stand-alone code for two primary reasons. First, the finite element mechanics of Diablo II allow for the modeling of the entire sputtering device instead of just the capsule and the inner chamber surfaces, which strengthens the tool's flexibility. Second, the setup of the code in an object-oriented manner allows for the feasible addition of a module representing the thermal modeling tool.

The input to the model includes the variables and their defaults in Table 1. The properties of the remainder of the chamber assembly are defined through the Diablo II input deck. Note that these defaults have no physical basis for their values, and will not necessarily reflect actual conditions. The user also provides the following:

- A pointwise load curve indicating various capsule positions during the transient simulation.
- Values of the chamber facets' view factors where no capsule is present, which may be found using LLNL's FACET code.
- Enclosure radiation emissivity curve values and wavelength breakpoints.
- Capsule material number. The materials are defined elsewhere in the Diablo II input deck.
- Number of surfaces.
- Chamber facets' heat transfer coefficients and adjacent chamber gas temperatures.
- Chamber facets' emissivity curve number, and whether or not they participate in conduction (i.e. an infinite blackbody).

It is stressed that under the current setup, the user MUST specify a Neumann load curve where the values of the load curve are equivalent to the time points. This allows for the module to access the current time during the simulation for purposes of determining capsule motion. The capsule motion algorithm operates in a manner similar to other traditional piecewise loading curves:

- For NumMotionPts = 1, the capsule is fixed at the position specified.
- If the current time is less than the first listed motion point time, then the capsule is set at the first listed motion point.
- If the current time is greater than the last listed motion point time, then the capsule is set at the last listed motion point
- If the current time is between two motion points, then a linear interpolation algorithm is used to determine the capsule position.

TABLE 1. Input Variables for the Thermal Modeling Tool.

Name	Description	Default value
Capsule Parameters		
CapsuleOuterRadius	Outer radius of film	5×10^{-4} m
CapsuleInnerRadius	Inner radius of film	0 m
CapsuleEmisCurve	Emissivity curve number of capsule	1
NumMotionPts	Number of load curve points to define capsule motion during the transient simulation	1
Contact Parameters		
ContactDistance	Maximum distance between center of capsule and surface to allow for contact calculation	6×10^{-4} m
ContactHTCoeff	Contact heat transfer coefficient	1.0 W/(m^2-K)
ContactArea	Contact area	10^{-7} m^2
ContactConvTol	Iterative contact convergence tolerance	0.001
MaxContactItns	Maximum allowable iterations in contact solution	10
CalcContact	Perform contact calculation?	Y
Convection Parameters		
CapsuleAdsHTCoeff	Capsule adsportion (convection) heat transfer coefficient to chamber gas	1.0 W/(m^2-K)
CapsuleGasTemperature	Chamber gas temperature at capsule surface	500 K
CalcAds	Perform convection calculation?	Y
Enclosure Radiation Parameters		
NumBands	Number of enclosure radiation bands	1
RadiationUnits	Radiation units type: "ENG" or "SI"	SI
NumEmisCurves	Number of emissivity curves	1
MaxRadItns	Maximum allowable iterations in enclosure radiation solution (multiple bands only)	10
RadConvTol	Iterative enclosure radiation convergence tolerance (multiple bands only)	0.001
CalcRad	Perform enclosure radiation calculation?	Y

Contact Algorithm Implementation

When the contact algorithm is called, the code implements three tests for contact for all facets. In this algorithm, all facets consist of four nodes (see Figure 1), and contact only occurs when all three tests are passed. The three tests are the following:

1. **Nodal distance cutoff**. For spherical capsules, contact is only possible if the center of the capsule is within some minimum distance to an arbitrary node in the facet. The capsule-Node 1 distance cannot be more than d_{max}, where

$$d_{max}^2 = d_{n,max}^2 + ContactDistance^2 \tag{1}$$

   and $d_{n,max}$ is the maximum distance between Node 1 and Nodes 2 through 4, and *ContactDistance* is listed in Table 1.

2. **Contact distance calculation**. The distance d between the center of the capsule and a facet plane is known by the relation

$$d = \frac{Ax_a + By_a + Cz_a + D}{\sqrt{A^2 + B^2 + C^2}} \tag{2}$$

   where $\mathbf{r}_a = (x_a, y_a, z_a)$ is the global coordinate position of the center of the capsule. The values of the coefficients are found by

$$
\begin{aligned}
A &= (y_2 - y_1)(z_3 - z_1) - (y_3 - y_1)(z_2 - z_1) \\
B &= (z_2 - z_1)(x_3 - x_1) - (z_3 - z_1)(x_2 - x_1) \\
C &= (x_2 - x_1)(y_3 - y_1) - (x_3 - x_1)(y_2 - y_1) \\
D &= -Ax_1 - By_1 - Cz_1
\end{aligned}
\tag{3}
$$

   where the subscripts 1, 2, and 3 denote three of the facet nodes. Note that all four nodes in each facet must be coplanar. Contact between the capsule and the facet is only possible if the distance d is less than the variable *ContactConvTol* in Table 1.

3. **Contact point calculation**. If the capsule has been found to be sufficiently close to the facet plane, then the location of the contact point in the facet plane is determined. The contact point is inside the facet if the isoparametric coordinates of the contact point are within the bounds of the four-node facet (i.e. both ξ and η must be between -1 and +1). The test begins by projecting the center of the capsule onto the facet plane using

$$\mathbf{r}_c = \mathbf{r}_a - d\mathbf{n} \tag{4}$$

   where $\mathbf{r}_c = (x_c, y_c, z_c)$ is the location of the contact point in global coordinates, and $\mathbf{n} = (A, B, C)$ is the planar norm. Next, a local coordinate system is declared

such that a chosen node is at the origin, an adjacent node in the facet is along the x-axis, and the facet plane is the local xy-plane. The local x and y positions of the nodes in the facet plane are

$$\tilde{x} = \sum_{i=1}^{4} N_i^e \tilde{x}_i^e$$
$$\tilde{y} = \sum_{i=1}^{4} N_i^e \tilde{y}_i^e$$

(5)

where $\tilde{x}_i^e$ and $\tilde{y}_i^e$ are the nodal positions in local coordinates, and N_i^e are the shape functions, which are found by

$$N_i^e(\xi,\eta) = \frac{1}{4}(1 + \xi_i\xi)(1 + \eta_i\eta), \; i = 1 \text{ to } 4$$

(6)

The isoparametric coordinates (ξ_c, η_c) of the projected contact point in local coordinates $(\tilde{x}_c, \tilde{y}_c, \tilde{z}_c = 0)$ are found by applying equation (5) for $\tilde{x}_c$ and $\tilde{y}_c$. The resultant expressions are

$$A_k^*\xi_c + B_k^*\eta_c + C_k^*\xi_c\eta_c + D_k^* = 0, \; k = (1, 2)$$

(7)

where for $k = 1$,

$$A_1^* = -\tilde{x}_1 + \tilde{x}_2 + \tilde{x}_3 - \tilde{x}_4$$
$$B_1^* = -\tilde{x}_1 - \tilde{x}_2 + \tilde{x}_3 + \tilde{x}_4$$
$$C_1^* = \tilde{x}_1 - \tilde{x}_2 + \tilde{x}_3 - \tilde{x}_4$$
$$D_1^* = -4\tilde{x}_c + \sum_{i=1}^{4} \tilde{x}_i$$

(8)

Equivalent expressions exist for $k = 2$ except the local y-coordinates are used in lieu of the local x-coordinates in equation (8). The isoparametric coordinates are solved by iteration, where the equations (7) are linearized for iteration $p+1$ using

$$A_k^*\xi_c^{p+1} + B_k^*\eta_c^{p+1} \approx D_k^* - C_k^*\xi_c^p\eta_c^p, \; k = (1, 2)$$

(9)

The values of $(\xi_c^{p+1}, \eta_c^{p+1})$ are then solved using Cramer's Rule. The iterations continue until

$$\left[\sum_{k=1}^{2} \left| A_k^*\xi_c^{p+1} + B_k^*\eta_c^{p+1} + C_k^*\xi_c^{p+1}\eta_c^{p+1} + D_k^* \right| \right] < ContactConvTol$$

(10)

9

If the code has determined that contact has taken place, then the stiffness matrices are updated accordingly. This implementation is described later in this report.

Enclosure Radiation Algorithm Description

The enclosure radiation algorithm used in the model is very similar to traditional enclosure radiation in finite element codes (e.g. TOPAZ3D), where the radiosity and irradiation on each facet is determined. For single-banded enclosure radiation, the radiosity J is found by solving the matrix equation

$$A_{ij}J_j = \sigma T_{avg,i}^4 \qquad (11)$$

where T_{avg} is the average facet temperature, σ is the Stefan-Boltzmann constant, and

$$A_{ij} = \frac{\delta_{ij}}{\varepsilon_i} - \frac{(1-\varepsilon_i)}{\varepsilon_i}F_{ij} \qquad (12)$$

where δ_{ij} is the Kronecker delta, ε_i is the emissivity of surface i, and F_{ij} is the view factor associated with radiation transfer from surface i to surface j. The irradiation G on a facet i is found using

$$G_i = F_{ij}J_j \qquad (13)$$

For multi-banded view factors, the irradiation and radiosity are iterated. The irradiation is calculated using equation (13), and the radiosity is calculated as

$$J_i = \varepsilon_i f_i \sigma T_{i,avg}^4 + (1-\varepsilon_i)G_i \qquad (14)$$

where f is the blackbody fraction for the band.

The parameter in equations (11) through (14) that is unique to this thermal model is the adjustment of the view factor matrix F_{ij} due to the position of the capsule. Although the view factors between the various facets in the capsule-free enclosure are known, the effect of the capsule on these view factors needs to be calculated. The capsule-facet view factors are calculated based on the equivalence of the view factor and the fraction of total solid angle occupied by the facet when viewed by the capsule. Figure 1 shows that the corners of the solid angle occupied by the facet intersects the four vectors $\mathbf{v}_1$, $\mathbf{v}_2$, $\mathbf{v}_3$, and $\mathbf{v}_4$. In addition, this rectangular area may be divided into two triangles by drawing a plane using $\mathbf{v}_1$ and $\mathbf{v}_3$. The calculation proceeds as follows:

- The cosines and sines of the facet angular lengths θ_{12}, θ_{23}, θ_{34}, θ_{41}, and θ_{31} are found using

$$\cos\theta_{ij} = \frac{\mathbf{v}_i \bullet \mathbf{v}_j}{|\mathbf{v}_i||\mathbf{v}_j|}$$

$$\sin\theta_{ij} = \sqrt{1 - \cos^2\theta_{ij}} \tag{15}$$

- The cosines of the dihedral angles are calculated from spherical trigonometry as

$$\cos\alpha_i = \left[\frac{\cos\theta_{jk} - \cos\theta_{ij}\cos\theta_{ik}}{\sin\theta_{ij}\sin\theta_{ik}}\right], \ (i, j, k) = \{1, 2, 3\} \tag{16}$$

$$\cos\beta_i = \left[\frac{\cos\theta_{jk} - \cos\theta_{ij}\cos\theta_{ik}}{\sin\theta_{ij}\sin\theta_{ik}}\right], \ (i, j, k) = \{1, 3, 4\} \tag{17}$$

- The capsule-facet view factor is then calculated as

$$F_{cap-i} = \frac{(\alpha_1 + \alpha_2 + \alpha_3 + \beta_1 + \beta_3 + \beta_4 - 2\pi)}{4\pi} \tag{18}$$

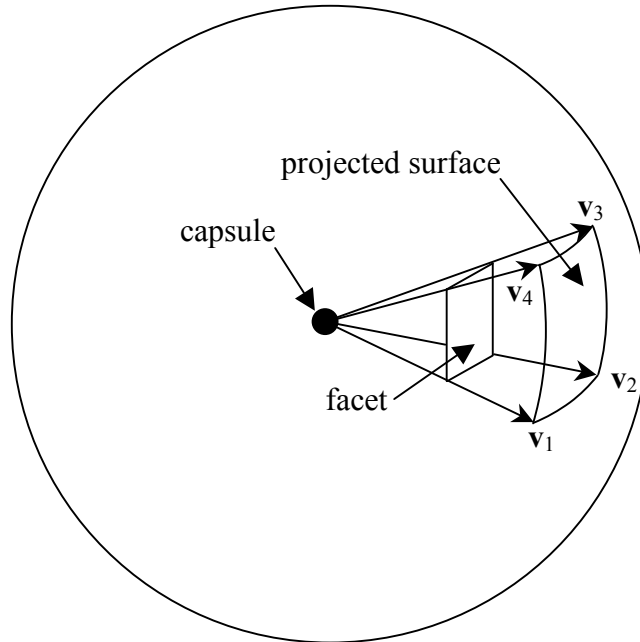The facet-capsule view factor may then be found using the reciprocity relation.

FIGURE 1. Projected surface used in determination of capsule-facet view factor.

The presence of the capsule also adjusts the facet-facet view factors. If the typical capsule dimension is assumed to be small compared to the facet dimensions, then the facet-facet view factors will most likely not be affected by the presence of the capsule. Therefore, the simplest way to adjust facet-facet view factors is to do the following for each facet i:

- Find the vector from the center of facet i to the center of the capsule.
- Loop through vectors between the centers of facet i and facet j to find the vector with the closest angle as the facet-capsule vector. This is the blocked view factor.
- If the blocked view factor is larger than the facet-capsule view factor, then subtract the facet-capsule view factor from the blocked view factor.
- If the blocked view factor is smaller than the facet-capsule view factor, then make the blocked view factor zero and repeat.

Finite Element Implementation

Enclosure bulk nodes represent a spherical capsule inside a radiation enclosure. This capsule may interact with any surface by either radiative transport, by surface contact, or via adsorption of chamber gases. The implementation of these three modes of heat transfer is now explained.

Contact

Contact heat transfer is handled in a way similar to a traditional bulk node. The contact heat transfer coefficient between a surface n and the bulk node is nonzero only when the node is within a distance from the surface. A point heat transfer area on the facet surface approximates the contact, where the net force vector (i.e. heat flow) on the facet surface is

$$
\begin{aligned}
\left(f_i\right)_{contact} &= -\int vq''dA = \int N_i h_{contact}(x,y)\left(T(x,y)-T_b\right)dA \\
&= -\sum_{j=1}^{4}\left[\int N_i h_{contact}\delta\left(\xi-\xi_c,\eta-\eta_c\right)N_j^T dA\right]\left(T_j-T_5\right) \\
&= -\sum_{j=1}^{4}\left[N_i\left(\xi_c,\eta_c\right)h_{contact}A_{contact}N_j\left(\xi_c,\eta_c\right)\right]\left(T_j-T_5\right) \qquad (19) \\
&= -\sum_{j=1}^{4}\left(K_{ij}\right)_{contact}\left(T_j-T_5\right) \\
&= -\sum_{j=1}^{4}\left(K_{ij}\right)_{contact}T_j + \sum_{j=1}^{4}\left(K_{ij}\right)_{contact}T_5
\end{aligned}
$$

where $h_{contact}$ is the contact heat transfer coefficient, $A_{contact}$ is the contact area, and K_{ij} is the stiffness matrix. This is equivalent to an external force vector of

$$\left(f_i\right)_{contact} = -\sum_{j=1}^{5}\left(K_{ij}\right)_{contact}T_j \, , \, i = 1 \text{ to } 4 \qquad (20)$$

where

$$\left(K_{i5}\right)_{contact} = -\sum_{j=1}^{4}\left(K_{ij}\right)_{contact} \qquad (21)$$

The stiffness matrix is found using

$$\left(K_{ij}\right)_{contact} = N_i\left(\xi_c,\eta_c\right)h_{contact}A_{contact}N_j\left(\xi_c,\eta_c\right), \, i = 1 \text{ to } 4, j = 1 \text{ to } 4. \qquad (22)$$

Similarly, the net force vector on the capsule is

$$\left(f_5\right)_{contact} = \int vq''dA = -\sum_{j=1}^{4}\int N_5 h_{contact}\left(T_5 - T_j\right)dA$$

$$= -\sum_{j=1}^{4}\left\{\left[\int N_5 h_{contact}N_j dA\right]T_5 - \left[\int N_5 h_{contact}N_j dA\right]T_j\right\} \qquad (23)$$

$$= -\sum_{j=1}^{4}\left(K_{5j}\right)_{contact}T_5 + \sum_{j=1}^{4}\left(K_{5j}\right)_{contact}T_j$$

Therefore, the elemental force vector of the capsule is increased by

$$\left(f_5\right)_{contact} = \sum_{j=1}^{5}\left(K_{5j}\right)_{contact}T_j \, , \, i = 1 \text{ to } 4 \qquad (24)$$

where

$$\left(K_{5j}\right)_{contact} = -\sum_{j=1}^{4}\left(K_{5j}\right)_{contact} \qquad (25)$$

The stiffness matrices for all chamber wall facets are computed at the beginning of each step (or only at the beginning of the first step if there is no capsule motion), and the internal force vector is calculated for every iteration.

Adsorption

A simple heat transfer coefficient relation may handle the energy adsorbed by the sputtered particles akin to convection. The elemental net force vector is thus

$$\left(f_i\right)_{ads} = \left(b_i\right)_{ads} - \sum_{j=1}^{5}\left(K_{ij}\right)_{ads}T_j \, , \, i = 1 \text{ to } 5 \qquad (26)$$

The stiffness matrix is found using

$$\left(K_{ij}\right)_{ads} = \int N_i h_{ads} N_j^T dA \,, \quad i = 1 \text{ to } 4. \tag{27}$$

for the walls and

$$\left(K_{5j}\right)_{ads} = \delta_{5j} h_{ads} A_b / N \tag{28}$$

for the capsule. In addition,

$$\left(b_i\right)_{ads} = \int N_i h_{ads} T_{gas} dA \,, \quad i = 1 \text{ to } 4. \tag{29}$$

for the walls and

$$\left(b_5\right)_{ads} = h_{ads} A_b T_{gas} / N \tag{30}$$

for the capsule, where A_b is the surface area of the capsule. The above relations for the walls are discretized as

$$\left(K_{ij}\right)_{ads} = dis \times \left\{ \sum_{iGauss=1}^{4} \left[N_i h_{ads} N_j \right]_{iGauss} \right\}, \quad i = 1 \text{ to } 4. \tag{31}$$

The stiffness matrices, and internal and external force vectors are determined each iteration for each block of 32 facets on the chamber walls.

Enclosure Radiation

The enclosure radiation portion of the bulk node incorporation is handled very similarly to a traditional enclosure radiation scheme with multi-banded view factors. The net amount of energy absorbed by a wall element facet from all surroundings is

$$\left(q_{net,total}\right)_n = A_n \left[\varepsilon_n G_n - f_n \varepsilon_n \sigma T_n^4 \right] \tag{32}$$

where f_n, ε_n, A_n, and G_n are the blackbody fraction, emissivity, surface area, and irradiation associated with facet n. A traditional enclosure implementation into finite element codes adjusts the above equation to yield

$$\left(q_{net,total}\right)_n = A_n \left[\left(3 f_n \varepsilon_n \sigma T_n^4 + \varepsilon_n G_n \right) - 4 f_n \varepsilon_n \sigma T_n^4 \right] \tag{33}$$

Therefore, for each wall facet, the force vector is

$$\left(f_i\right)_{er} = \left(b_i\right)_{er} - \sum_{j=1}^{5} \left(K_{ij}\right)_{er} T_j \tag{34}$$

where

$$\left(b_i\right)_{er} = \int N_i\left(3f_n\varepsilon_n\sigma T_n^4 + \varepsilon_n G_n\right)dA_n$$

$$\left(K_{ij}\right)_{er} = \begin{cases} \int N_i\left(4f_n\varepsilon_n\sigma T_n^3\right)N_j^T dA_n, & i < 5 \\ 0, & i = 5 \end{cases}$$

(35)

If the approximation $T_i = T_j$ is used (as in the TOPAZ code FE enclosure radiation implementation), then the discretization follows

$$\left(b_i\right)_{er} = dis \times \left\{ \sum_{iGauss=1}^{4}\left[N_i\left(3f_n\varepsilon_n\sigma T_n^4 + \varepsilon_n G_n\right)\right]_{iGauss} \right\}$$

$$\left(K_{ij}\right)_{er} = dis \times \left\{ \sum_{iGauss=1}^{4}\left[\delta_{ij}N_i\left(4f_n\varepsilon_n\sigma T_n^3\right)N_j\right]_{iGauss} \right\}$$

(36)

where *dis* is the discriminant for that surface. The amount of heat gained by the capsule from a wall facet is

$$\left(q_{net,cap-wall}\right)_n = A_b F_{bn}\left(J_n - J_b\right)$$

(37)

where F_{bn} is the capsule-facet view factor, and J_n and J_b are the facet and capsule radiosities, respectively. Note that in the above equations the irradiation and radiosity are band-dependent and are not multiplied by f_n. The total amount of heat gained by the capsule from N facets is

$$q_{net,cap-wall} = \sum_{n=1}^{N} A_b F_{bn}\left(J_n - J_b\right)$$

(38)

The force vector for the capsule is thus

$$\left(f_5\right)_{er} = \left(b_5\right)_{er} = A_b F_{bn}\left(J_n - J_b\right)$$

(39)

for each wall facet.

The stiffness matrices, and internal and external force vectors are determined for each iteration for each block of 32 facets on the chamber walls.

Algorithm Verification

Two sets of six simulations were run to verify the correct implementation of the aforementioned algorithm. In these simulations, the entire capsule was assumed to be comprised of the film (i.e. the inside capsule radius was set to zero). Figure 2 shows the

15

two arrangements used in the tests: one set of simulations used a six-facet enclosure, while the other set used a 54-facet enclosure. The reason for performing tests on two sets is to check for equivalence of results, which suggests the algorithm is unaffected by the blocking structure used in Diablo II.

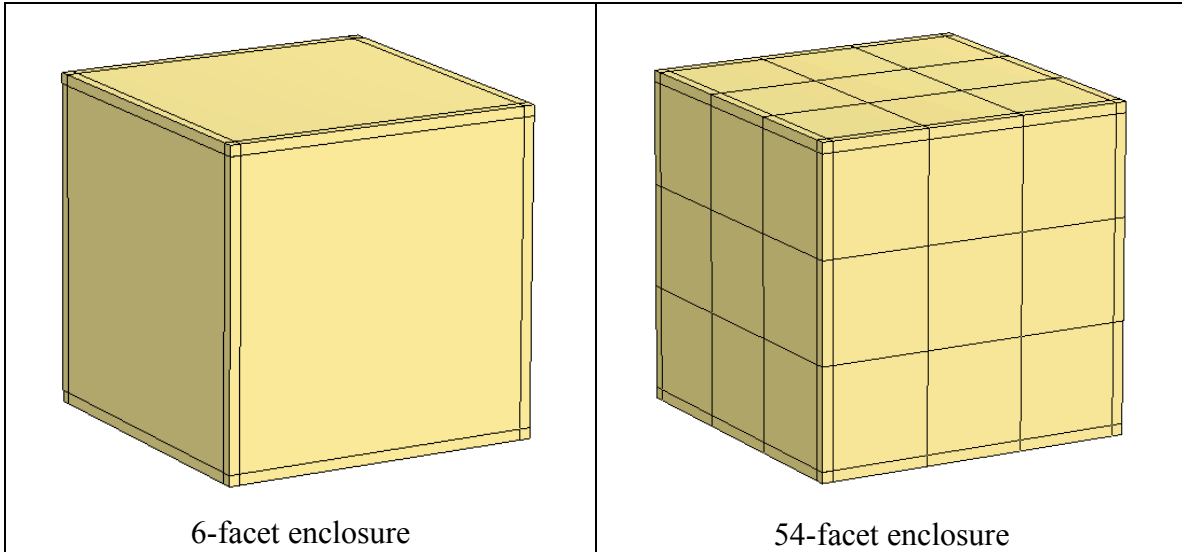| 6-facet enclosure | 54-facet enclosure |

FIGURE 2. Simulation domains used in verifications tests.

In these simulations, various aspects of heat transfer were turned on or off for analysis of their individual components, and then a final verification problem incorporated all heat transfer components. In addition, a multi-banded radiation enclosure problem was run to ensure equivalence with the single-banded approach. The simulation domain featured a cubic chamber space of dimensions 0.28m × 0.28m, and all chamber walls contained a thickness of 0.01m. The capsule position was fixed at the $z = 0.01$m surface at the location indicated below in Figure 3:
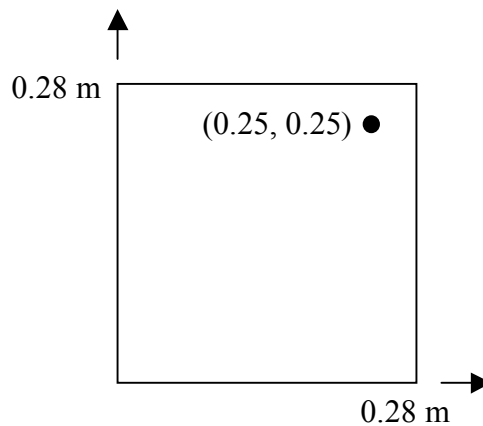

FIGURE 3. Simulation domain setup for verification runs.

16

In these tests, the capsule temperature was initialized at $T_{b,i} = 300$ K. In addition, the material properties of the capsule are assumed to be independent of temperature and are approximations for Beryllium. The chamber walls contained an emissivity of 1.0. The chamber walls were made thin, and all outer surfaces of the box were kept at 500 K, which resulted in nearly constant internal chamber wall temperature of 500 K throughout the simulation. The resultant temperature change of the facet surfaces was less than 0.1 K for all simulation runs. The ODE describing the transient temperature of the capsule with time for these simulations is

$$m_b C_p \frac{dT_b}{dt} = h_c A_c \left(T_w - T_b\right) + h_{ads} A_b \left(T_{gas} - T_b\right) + \varepsilon_b \sigma A_b \left(T_w^4 - T_b^4\right) \tag{40}$$

where m_b and ε_b are the mass and emissivity of the capsule, σ is the Stefan-Boltzmann constant, A_c and A_b are the contact and capsule surface area, and T_w is the capsule wall temperatures and is assumed to be constant in time at 500 K. The first, second, and third terms on the right-hand side of equation (40) are the contribution due to contact with the chamber walls, gas adsorption, and enclosure radiation, respectively. The linearity of the contact and adsorption terms allows for an exact solution when no radiation is present:

$$\frac{T_w - T_b(t)}{T_w - T_{b,i}} = \exp\left(-\frac{h_c A_c}{m_b C_p} t\right), \text{ contact only (Test 2)} \tag{41}$$

$$\frac{T_{gas} - T_b(t)}{T_{gas} - T_{b,i}} = \exp\left(-\frac{h_{ads} A_b}{m_b C_p} t\right), \text{ adsorption only (Test 3)} \tag{42}$$

Inclusion of enclosure radiation makes equation (40) nonlinear, and hence it must be solved using a finite difference discretization as

$$T_b^{p+1} = T_b^p + \frac{\varepsilon_b \sigma A_b \Delta t}{m_b C_p}\left[T_w^4 - \left(T_b^p\right)^4\right], \text{ radiation only (Tests 4 and 5)} \tag{43}$$

$$
\begin{aligned}
T_b^{p+1} = {} & \left[1 - \frac{h_c A_c \Delta t}{m_b C_p} - \frac{h_{ads} A_b \Delta t}{m_b C_p}\right] T_b^p + \frac{h_c A_c \Delta t}{m_b C_p} T_w \\
& + \frac{h_{ads} A_b \Delta t}{m_b C_p} T_{gas} + \frac{\varepsilon_b \sigma A_b \Delta t}{m_b C_p}\left[T_w^4 - \left(T_b^p\right)^4\right]
\end{aligned}
$$

, all modes of heat transfer (Test 6)

$$\tag{44}$$

The values of the parameters used in the simulations are

$$\rho_b = 1850 \, ^{kg}\!\!/\!_{m^3}$$

$$C_p = 2000 \, ^{J}\!\!/\!_{kg-K}$$

$$h_{ads} = 100.0 \, ^{W}\!\!/\!_{m^2-K}$$

$$h_c = 100.0 \, ^{W}\!\!/\!_{m^2-K}$$

$$A_c = 0.001 m^2 \tag{45}$$

$$D_b = 0.01 m$$

$$\varepsilon_b = 0.7$$

$$\Delta t = 0.1 sec$$

$$T_{b,i} = 300K$$

$$T_w = T_{gas} = 500K$$

where ρ_b and D_b are the mass density and diameter of the spherical capsule, respectively. The simulations were run for 200 steps for a final time of 20 seconds. Tables 2 and 3 clearly shows that the simulated final capsule temperature values agreed with those determined using analytical or finite difference methods within less than 1%, which suggests that the implementation of the algorithm is correct.

TABLE 2. Results of Verification Tests for the 6-Surface Enclosure

Test	X = heat transfer mode used			Capsule Temperature Change (K) at t = 20 seconds			
	Contact	Adsorption	Radiation	Simulation	Analytical	Finite Difference	% error
1				0.00	0.00		0.00
2	X			128.55	128.77		0.17
3		X		55.28	55.40		0.22
4			X (single band)	6.94		6.95	0.14
5			X (multi-band)	6.94		6.95	0.14
6	X	X	X (single band)	150.65		150.88	0.15

TABLE 3. Results of Verification Tests for the 54-Surface Enclosure

Test	X = heat transfer mode used			Capsule Temperature Change (K) at t = 20 seconds			
	Contact	*Adsorption*	*Radiation*	*Simulation*	*Analytical*	*Finite Difference*	*% error*
1				0.00	0.00		0.00
2	X			128.48	128.77		0.23
3		X		55.28	55.40		0.22
4			X (single band)	6.94		6.95	0.14
5			X (multi-band)	6.94		6.95	0.14
6	X	X	X (single band)	150.59		150.88	0.19

Further tests were run regarding capsule motion. These tests verified the following:
- The rate of heat transfer to the capsule is independent of position for adsorption.
- For an enclosure where all walls contain the same temperature, the rate of heat transfer to the capsule is independent of position.
- Contact heat transfer between the capsule and chamber walls when the center of the capsule is within the specified contact distance

Tables 2 and 3 show that contact heat transfer dominates for this specific setup. Therefore, tests should indicate that the rate of capsule temperature rise should drop if the capsule is lifted off of the wall. Figure 4 shows capsule temperature histories for various contact times. In these simulations, the capsule is initially positioned on the wall surface, but is then lifted after the times shown. The figure confirms that the heat gain by the capsule is reduced when the capsule is removed from the chamber wall surface.
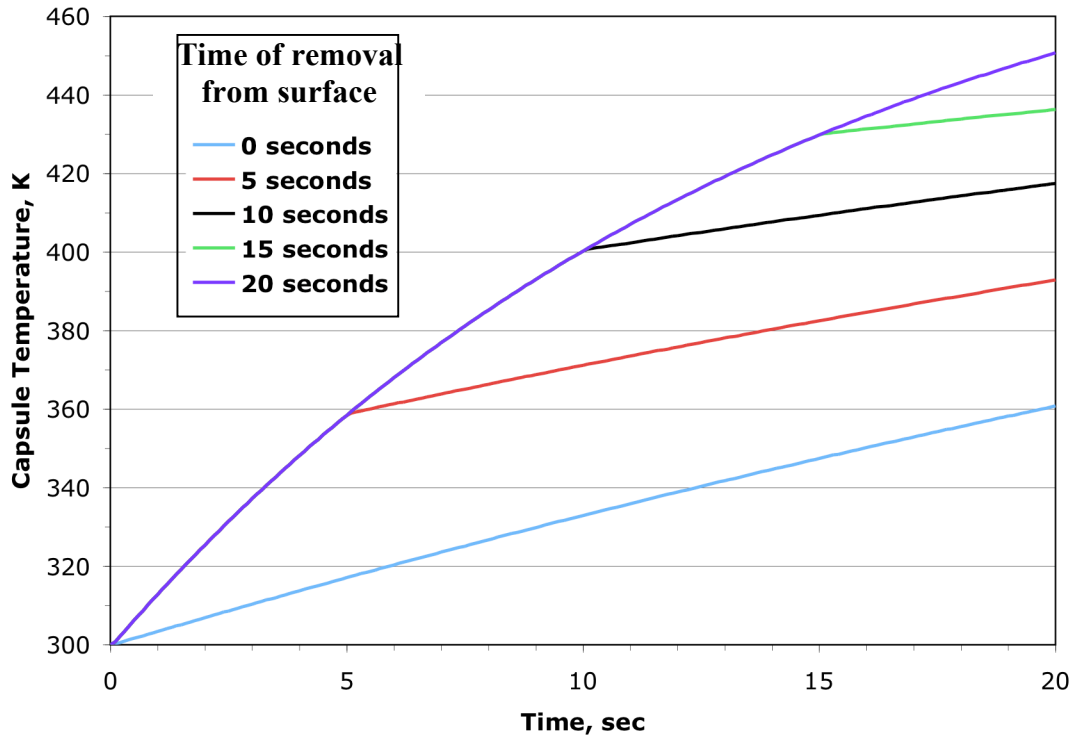
FIGURE 4. Temperature history of capsule for various durations of contact with the chamber wall surface.

Conclusions

A lumped capacitance model of a spherical capsule inside a sputtering chamber has been implemented, and tests have shown the correct thermal behavior of the system for the modes of heat transfer shown. However, questions remain regarding the values of input parameters to the module and whether additional or alternate modes of heat transfer should be implemented to improve the accuracy of the model. Fortunately, the current setup of the code allows for straightforward additions of other heat transfer modes to compliment the current availability. A good future direction of the effort should be to compare a simulated capsule thermal response to experimentally measured results for the purpose of obtaining reasonable input parameters.

Acknowledgements

References

1. Thornton, J. A. (1974) Influence of Apparatus Geometry and Deposition Conditions on the Structure and Topography of Thick Sputtered Coatings, *J. Vac. Sci. Technol.* **11**, 666-670.
2. Communications with Rich London (AX Division, LLNL).